

## Theoretical Investigations of CO<sub>2</sub> and H<sub>2</sub> Sorption in an Interpenetrated Square-Pillared Metal-Organic Material

Tony Pham,<sup>†,§</sup> Katherine A. Forrest,<sup>†,§</sup> Keith McLaughlin,<sup>†</sup> Brant Tudor,<sup>†</sup> Patrick Nugent,<sup>†</sup> Adam Hogan,<sup>†</sup>  
Ashley Mullen,<sup>†</sup> Christian R. Cioce,<sup>†</sup> Michael J. Zaworotko,<sup>†</sup> and Brian Space<sup>\*,†</sup>

<sup>†</sup>*Department of Chemistry, University of South Florida,  
4202 E. Fowler Ave., CHE205, Tampa, FL 33620-5250*

<sup>§</sup>Authors contributed equally

\*brian.b.space@gmail.com

(Dated: Submitted on March 19, 2013)

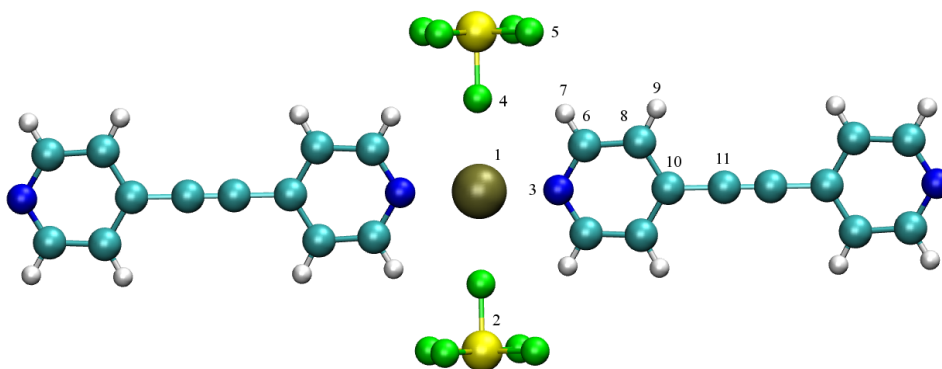
### Atomic Partial Point Charges

Stationary electrostatic interactions were modeled using atomic point partial charges that are localized on the atomic positions of each atom. Examination of the unit cell for [Cu(dpa)<sub>2</sub>SiF<sub>6</sub>-i] revealed 11 atoms in chemically distinct environments (Figure 1). The point partial charges were determined from electronic structure calculations on several gas phase fragments that mimic the chemical environment of the MOM. Note, it was shown that periodic fitting of the entire crystal structure was a more appealing alternative to obtain partial charges.<sup>1-3</sup> However, [Cu(dpa)<sub>2</sub>SiF<sub>6</sub>-i] contains atoms that are buried within the unit cell and this makes the charge fitting procedure rather difficult to obtain sensible partial charges.

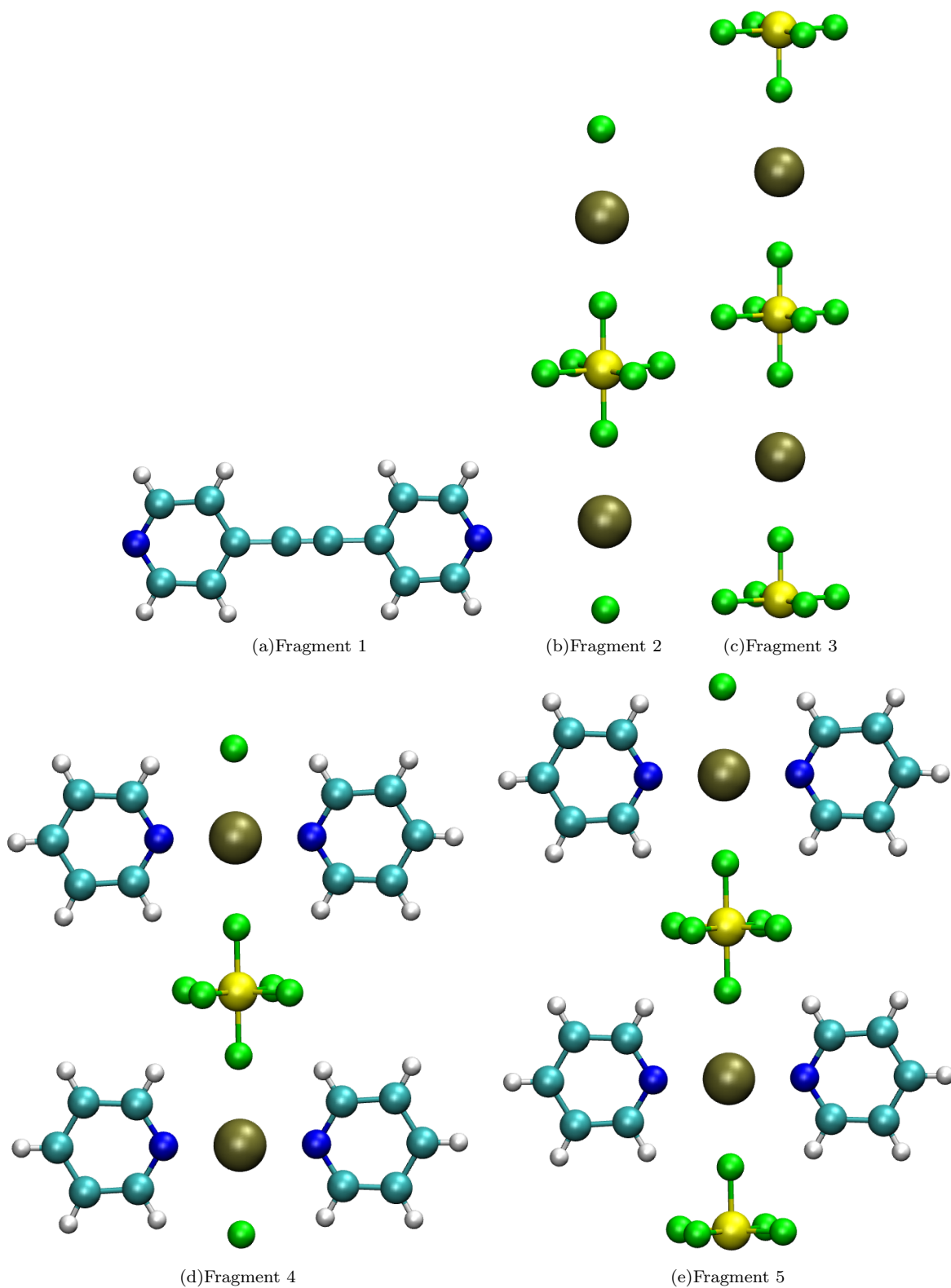
The NWChem<sup>4</sup> *ab initio* simulation package was used to perform the Hartree-Fock quantum mechanical calculations. All C, H, N, F, and Si atoms were treated with the 6-31G\* basis set. This basis set accounts for over-polarized charges that are appropriate for condensed phase simulations.<sup>3,5-8</sup> For the Cu<sup>2+</sup> ions, the LANL2DZ<sup>9-11</sup> effective core potential basis set was used to treat the inner electrons of the many-electron species. For the purposes of charge fitting, fragments of [Cu(dpa)<sub>2</sub>SiF<sub>6</sub>-i] were selected in a variety of ways to assess the effects of structural truncation on the fit charges. The addition of hydrogen atoms, where appropriate, was required for chemical termination of the fragment boundaries.

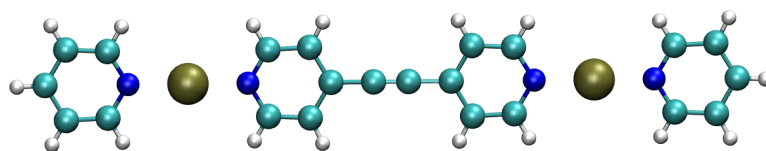
The CHELPG method<sup>12,13</sup> was used to perform the least-squared fit on the gas phase fragments. The partial charges for the chemically distinct atoms were in good agreement among the chosen fragments (Figure 2) For each unique atom, the charges were averaged between the fragments and were assigned the point charge of the corresponding nuclear center of the atom. Note, for each fragment, the terminal and buried atoms were not included in the averaging. The average partial charges for each fragment are shown in Table 1. The final tabulated partial charges for each chemically distinct atom in [Cu(dpa)<sub>2</sub>SiF<sub>6</sub>-i] can be found in Table 3. Based on the agreement between the fragments, these partial charges are accurate to within 0.1 electron units.

**Figure 1.** Chemically distinct atoms in [Cu(dpa)<sub>2</sub>SiF<sub>6</sub>-i] as referred to in Table 1 and 3. Atom colors: C = cyan, H = white, N = blue, F = green, Si = yellow, Cu = tan.

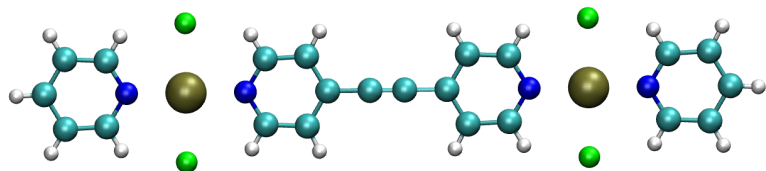


**Figure 2.** Fragments of  $[\text{Cu}(\text{dpa})_2\text{SiF}_6\text{-i}]$  that were selected for gas-phase charge fitting. Atom colors: C = cyan, H = white, N = blue, F = green, Si = yellow, Cu = tan.

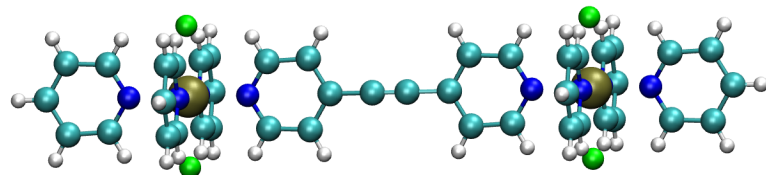




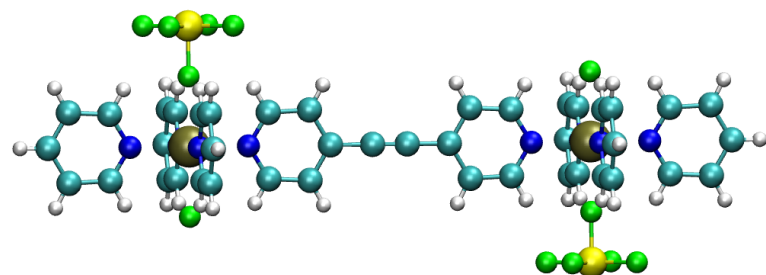
(f) Fragment 6



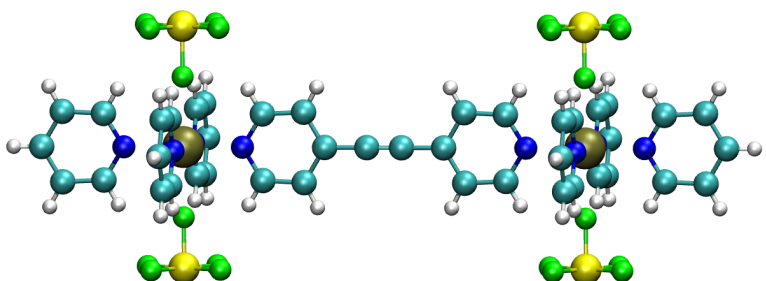
(g) Fragment 7



(h) Fragment 8



(i) Fragment 9



(j) Fragment 10

**Table 1.** Comparison of partial charges ( $e^-$ ) for a series of fragments as listed in Figure 2. Labeling of the atoms correlates to Figure 1.

Atom	Label	Frag 1	Frag 2	Frag 3	Frag 4	Frag 5	Frag 6	Frag 7	Frag 8	Frag 9	Frag 10
Cu	1	-	-	-	0.2803	0.3411	0.2262	-	0.2847	0.3632	-
Si	2	-	1.5471	1.7753	1.7040	1.6762	-	-	-	-	-
N	3	-	-	-	-0.0753	-0.0561	-0.0686	-0.0019	-0.0658	-0.0752	-
F	4	-	-	-0.6166	-0.4212	-0.4798	-	-0.6020	-	-0.5512	-
F	5	-	-	-	-0.5872	-0.5616	-	-	-	-0.5492	-0.5529
C	6	-	-	-	0.2027	0.1247	-	0.1602	0.1475	0.1150	0.1118
H	7	-	-	-	0.1368	0.1726	0.1338	0.1471	0.1701	0.1789	0.2034
C	8	-	-	-	-0.3461	-0.2690	-0.2801	-0.3737	-0.3570	-0.2995	-0.2583
H	9	0.2408	-	-	0.1849	0.1729	0.1509	0.1877	0.1892	0.1847	0.1613
C	10	-	-	-	-	-	-	-	0.2863	0.2440	0.2041
C	11	-	-	-	-	-	-	-0.1545	-0.1682	-0.1484	-

### Many-Body Polarization

Many-body polarization was explicitly included in the simulations by use of a Thole-Applequist type model.<sup>14–16</sup> An overview of the model used in this work is given here. Consider a static electric field applied to a system of  $N$  atomic sites. The induced dipole  $\vec{\mu}_i$  at each site  $i$  is calculated *via* the following:

$$\vec{\mu}_i = \alpha_i^\circ \left( \vec{E}_i^{stat} + \vec{E}_i \right) \quad (1)$$

where  $\alpha^\circ$  is a scalar atomic point polarizability,  $\vec{E}^{stat}$  is the electrostatic field vector due to the atomic point partial charges of the MOM atoms and the sorbate molecules, and  $\vec{E}$  is the field due to the atomic induced dipoles. Rewriting equation 1 in terms of the dipole field tensor  $\hat{\mathbf{T}}_{ij}$ , one obtains the following:

$$\vec{\mu}_i = \alpha_i^\circ \left( \vec{E}_i^{stat} - \sum_{j \neq i}^N \hat{\mathbf{T}}_{ij} \vec{\mu}_j \right) \quad (2)$$

In this work, the following dipole field tensor is used:

$$\hat{T}_{ij}^{\alpha\beta} = \nabla^\alpha \nabla^\beta \left( \frac{s(r)}{r_{ij}} \right) \quad (3)$$

where the screening function  $s(r) = \left(\frac{\lambda r}{2} + 1\right)e^{-\lambda r}$  serves to describe the charge distributions of the interacting dipoles. The damping parameter  $\lambda$  is set to 2.1304, consistent with work done by Thole and others, eliminating the short range divergences that occur in the polarization model when dealing with point dipoles (known as the polarization catastrophe).<sup>15,17,18</sup>

Although matrix inversion may be used to find an exact solution to the self-consistent field problem (equation 2), iterative methods can produce a solution in a fraction of the computation time and are extremely stable when Gauss-Seidel relaxation is employed.<sup>19</sup> Initially, every induced dipole vector in the system is evaluated as

$$\vec{\mu}_i = \alpha_i^\circ \vec{E}_i^{stat} \quad (4)$$

On each subsequent iteration  $\xi$ , the dipole field tensor is written as a sum of its lower triangular and strictly upper triangular components  $\hat{\mathbf{T}} \equiv \hat{\mathbf{T}}^L + \hat{\mathbf{T}}^U$ , and each dipole is updated sequentially *via* forward substitution

$$\vec{\mu}_i^\xi = \alpha_i^\circ \left( \vec{E}_i^{stat} - \sum_{i>j} \hat{\mathbf{T}}_{ij}^L \vec{\mu}_j^{\xi+1} - \sum_{i<j} \hat{\mathbf{T}}_{ij}^U \vec{\mu}_j^\xi \right) \quad (5)$$

Finally, the polarization energy for the MOM–sorbate system is calculated by the following based on the work of Palmo and Krimm<sup>20</sup> using the  $\xi^{\text{th}}$  iteration dipoles and the  $(\xi + 1)^{\text{th}}$  induced field

$$U_{pol}^\xi = -\frac{1}{2} \sum_i \vec{\mu}_i^\xi \cdot \vec{E}_i^{stat} - \frac{1}{2} \sum_i \vec{\mu}_i^\xi \cdot \vec{E}_i^{\xi+1} \quad (6)$$

### Atomic Point Polarizability

Many-body polarization was modeled using atomic point polarizabilities. The values for C, H, N, and F were parameterized in the work of van Duijnen *et al.*,<sup>18</sup> and were used in this study. This set of polarizability parameters was found to be highly transferable.<sup>3,6,8,14,18,21,22</sup> The parameter for Cu was determined in earlier work on PCN-61,<sup>8</sup> and was also used in this work. The atomic point polarizability value for Si was not previously parameterized for, and thus, it was calculated in this study.

To determine the atomic point polarizability value for Si, the polarizability tensor for gas phase  $\text{SiF}_6^{2-}$  (Figure 3) was calculated using the Q-Chem<sup>23</sup> *ab initio* simulation package with the aug-cc-pVDZ basis set. Afterwards, the Si parameter was then adjusted such that the molecular polarizability tensor, as calculated by the Thole-Applequist model<sup>14-16</sup>, was in good agreement to the tensor that was produced through *ab initio* calculations. For this calculation, the atomic point polarizability for all F atoms were assigned the fluorine value as parameterized by van Duijnen *et al.*<sup>18</sup> This derived molecular polarizability tensor was calculated using the Massively Parallel Monte Carlo (MPMC) code.<sup>24</sup> The polarizability tensors comparing *ab initio* results to those fit using the Thole-Applequist model is shown in Table 2. The fitted polarizability value for Si is shown in Table 3.

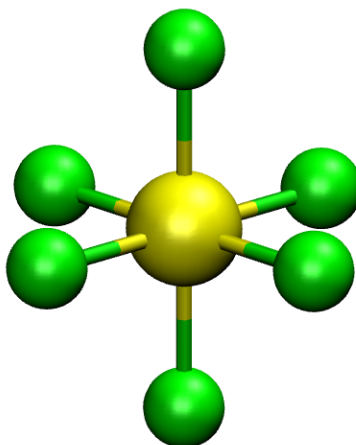


**Figure 3.** Gas phase  $\text{SiF}_6^{2-}$  used to calculate the atomic point polarizability of Si. Atom colors: F = green, Si = yellow.

**Table 2.** Polarizability tensors comparing *ab initio* results to those fit using the Thole-Applequist model for  $\text{SiF}_6^{2-}$ . The fitted polarizability value for Si is found in Table 3.

<i>ab initio</i>			Thole-Applequist		
4.592	0.001	-0.000	4.523	-0.000	-0.000
0.001	4.520	0.000	-0.000	4.554	-0.000
-0.000	0.000	4.520	-0.000	-0.000	4.554

**Table 3.** Molecular simulation parameters for  $[\text{Cu}(\text{dpa})_2\text{SiF}_6\text{-i}]$ . Label of atoms corresponds to Figure 1.

Atom	Label	$\epsilon(\text{K})$	$\sigma(\text{\AA})$	$q(e^-)$	$\alpha^\circ(\text{\AA}^3)$
Cu	1	2.51600	3.11400	0.28930	2.19630
Si	2	202.29000	3.82640	1.75079	2.13300
N	3	85.60000	3.25000	-0.05720	0.97157
F	4	25.16000	2.99700	-0.53420	0.44475
F	5	25.16000	2.99700	-0.56270	0.44475
C	6	35.25000	3.55000	0.14510	1.28860
H	7	15.11000	2.42000	0.15800	0.41380
C	8	35.25000	3.55000	-0.32090	1.28860
H	9	15.11000	2.42000	0.17810	0.41380
C	10	35.25000	3.55000	0.25390	1.28860
C	11	35.25000	3.55000	-0.15700	1.28860

### Grand Canonical Monte Carlo

All simulations of gas sorption and separation in  $[\text{Cu}(\text{dpa})_2\text{SiF}_6\text{-i}]$  were performed using Grand canonical Monte Carlo (GCMC) on a  $2 \times 2 \times 2$  unit cell system of the MOM. In this method, the chemical potential, volume, and temperature are held fixed while other statistical mechanical quantities (e.g. particle number) were allowed to fluctuate.<sup>25</sup> The simulation involves randomly inserting, deleting, translating, or rotating a sorbate molecule with acceptance or rejection based on a random number generator scaled by the energetic favorability of the move. An infinitely extended crystal environment was approximated by periodic boundary conditions with a spherical cutoff of 8.092 Å, which corresponds to half the shortest system cell dimension length. The average particle number was calculated by the following expression:<sup>26,27</sup>

$$\langle N \rangle = \frac{1}{\Xi} \sum_{N=0}^{\infty} e^{\beta\mu N} \left\{ \prod_{i=1}^{3N} \int_{-\infty}^{\infty} dx_i \right\} N e^{-\beta U(x_1, \dots, x_{3N})} \quad (7)$$

where  $\Xi$  is the grand canonical partition function,  $\beta$  is the quantity  $1/kT$  ( $k$  is the Boltzmann constant,  $T$  is the temperature),  $\mu$  represents the chemical potential of the gas reservoir, and  $U$  is the total potential energy. The chemical potential for  $\text{CO}_2$  was determined for a range of temperatures through the Peng-Robinson equation of state.<sup>28</sup> For  $\text{H}_2$ , the chemical potential was determined through the BACK equation of state.<sup>29</sup> The total potential energy of the MOM-sorbate system is calculated by:

$$U = U_{rd} + U_{es} + U_{pol} \quad (8)$$

where  $U_{rd}$  is the repulsion/dispersion energy through use of the Lennard-Jones potential,  $U_{es}$  is the electrostatic energy calculated by Ewald summation,<sup>1,30,31</sup> and  $U_{pol}$  is the polarization energy which is calculated using equation 6. For simulations that do not include explicit polarization,  $U_{pol}$  is equal to 0. For all simulations involving hydrogen sorption at 77 K, quantum mechanical dispersion effects were included semiclassically through the fourth order Feynman-Hibbs correction according to the following equation:<sup>32</sup>

$$U_{FH} = \frac{\beta\hbar^2}{24\mu} \left( U'' + \frac{2}{r} U' \right) + \frac{\beta^2\hbar^4}{1152\mu^2} \left( \frac{15}{r^3} U' + \frac{4}{r} U''' + U'''' \right) \quad (9)$$

where  $\hbar$  is the reduced Planck's constant and the primes indicate differentiation with respect to pair separation  $r$ .

The MOM-sorbate system was also treated with long-range corrections to all terms of the potential due to the finite size of the simulation box. The long-range contribution to the Lennard-Jones potential was calculated by:<sup>33</sup>

$$U_{LJ}^{LRC} = \frac{16\pi}{3V} \sum_{i=0}^{N-1} \sum_{j=0}^{N-1} \epsilon_{ij} \left( \frac{\sigma_{ij}^9}{3R_c^9} - \frac{\sigma_{ij}^3}{R_c^3} \right) \quad (10)$$

where  $r_{ij}$  is the distance between sites  $i$  and  $j$ ,  $\epsilon_{ij}$  and  $\sigma_{ij}$  are Lorentz-Berthelot mixed Lennard-Jones parameters,  $V$  is the volume of the simulation box, and  $R_c$  is the cut-off distance, which is set to one-half the shortest simulation box length (8.092 Å).

Long-range electrostatic interactions were handled by performing full Ewald summation. The long-range correction to the polarization energy was performed by replacing the static electric field with the shifted-field formula according to Wolf *et al.*,<sup>1,31,34</sup> which is the following:

$$\vec{E}_i^{shift} = \sum_j^{N-1} q_j \left( \frac{1}{r_{ij}^2} - \frac{1}{R_c^2} \right) \hat{r} \quad (11)$$

where  $q$  is the atomic point partial charge and  $\hat{r}$  is the radial unit vector.

In GCMC, the isosteric heats of adsorption,  $Q_{st}$ , were calculated based on the fluctuations of the number of particles,  $N$ , and total potential energy,  $U$ , in the system *via* the following expression:<sup>35</sup>

$$Q_{st} = - \frac{\langle NU \rangle - \langle N \rangle \langle U \rangle}{\langle N^2 \rangle - \langle N \rangle^2} + kT \quad (12)$$

Furthermore, the isothermal compressibilities,  $\beta_T$ , were calculated based on the fluctuations of the particle number through the following expression:<sup>35</sup>

$$\beta_T = \frac{V}{kT} \frac{\langle N^2 \rangle - \langle N \rangle^2}{\langle N \rangle^2} \quad (13)$$

For all state points considered, the simulations consisted of  $1 \times 10^7$  Monte Carlo steps to guarantee equilibration, followed by an additional  $1 \times 10^7$  steps to sample the desired thermodynamic properties. Simulations involving many-body polarization utilized a correlation time of  $1 \times 10^4$  steps. All simulations were performed using the Massively Parallel Monte Carlo (MPMC) code,<sup>24</sup> which is currently available for download on Google Code.

### CO<sub>2</sub> Models

Two potential energy functions for CO<sub>2</sub> have been developed for the accurate simulation of CO<sub>2</sub> sorption in heterogeneous systems: one that includes van der Waals and explicit charge-quadrupole interactions, referred to as CO<sub>2</sub>-PHAST; and one that includes van der Waals, charge-quadrupole, and explicit many-body polarization interactions, referred to as CO<sub>2</sub>\*-PHAST. The parameters for the two CO<sub>2</sub> potentials can be found in Table 4.

CO<sub>2</sub>-PHAST is a rigid five-site model that includes partial charges on the carbon and oxygen atoms of the CO<sub>2</sub> molecule. The partial charges represent the molecular quadrupole for CO<sub>2</sub>. Lennard-Jones parameters are located on the carbon atom and two off-atomic sites extending 1.091 Å away from the carbon atom. This model reproduces bulk CO<sub>2</sub> pressure-density data and is capable of describing correct sorption behavior in nonpolar MOMs where induced dipole energetics are negligible.

CO<sub>2</sub>\*-PHAST is an analogue of the previous model with atomic point polarizabilities located on the carbon and oxygen atoms of the CO<sub>2</sub> molecule. The atomic point polarizabilities represent the molecular polarizability tensor of CO<sub>2</sub>. For this model, the Lennard-Jones parameters are located on the carbon atom and the off-atomic positions that are localized 1.208 Å from the carbon atom. This model reproduces bulk CO<sub>2</sub> data and is capable of accurately describing sorption in charged/polar MOMs where many-body polarization interactions are essential.

Figure 4 shows the bulk CO<sub>2</sub> pressure-density isotherms for the two CO<sub>2</sub> models compared to experimental data<sup>36</sup> at 298 K and 273 K and pressures up to 10.0 atm. The pressure-density isotherms were determined from Grand canonical Monte Carlo (GCMC) simulations using the MPMC code.<sup>24</sup> For this, the average density was calculated by:

$$\langle \rho \rangle = \frac{\langle N \rangle}{V} \quad (14)$$

where  $\langle N \rangle$  is defined in the Grand Canonical Monte Carlo section. The isotherms for the two CO<sub>2</sub> potentials were in excellent agreement with the experimental data at both temperatures, thus validating the accuracy of these potentials in the bulk environment for the given pressure range.

**Table 4.** Parameters used to characterize the CO<sub>2</sub>-PHAST and CO<sub>2</sub>\*-PHAST CO<sub>2</sub> models. OA refers to the off-atomic sites.

Model	Atomic Site	$r(\text{Å})$	$\epsilon(\text{K})$	$\sigma(\text{Å})$	$q(e^-)$	$\alpha^\circ(\text{Å}^3)$
CO <sub>2</sub> -PHAST	C	0.00000	8.52238	3.05549	0.77106	0.00000
	O	1.16200	0.00000	0.00000	-0.38553	0.00000
	O	-1.16200	0.00000	0.00000	-0.38553	0.00000
	OA	1.09100	76.76607	2.94473	0.00000	0.00000
	OA	-1.09100	76.76607	2.94473	0.00000	0.00000
CO <sub>2</sub> *-PHAST	C	0.00000	19.61757	3.30366	0.77134	1.22810
	O	1.16200	0.00000	0.00000	-0.38567	0.73950
	O	-1.16200	0.00000	0.00000	-0.38567	0.73950
	OA	1.20800	46.47457	2.99429	0.00000	0.00000
	OA	-1.20800	46.47457	2.99429	0.00000	0.00000

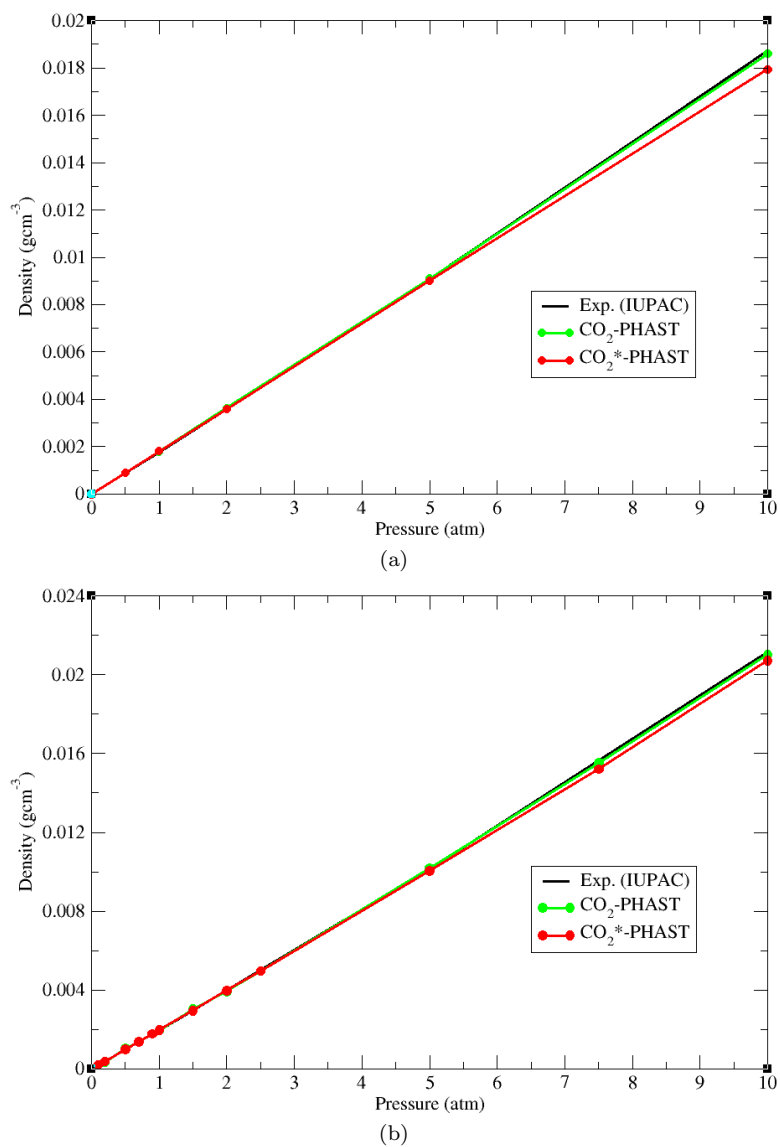


**Figure 4.** Pressure-density isotherms of CO<sub>2</sub> at (a) 298 K and (b) 273 K for the CO<sub>2</sub>-PHAST and CO<sub>2</sub>\*-PHAST CO<sub>2</sub> models compared to experiment at pressures up to 10.0 atm.

## H<sub>2</sub> Models

Three hydrogen potentials were used in the simulations presented in this work. The first of these, denoted Buch,<sup>37</sup> is a single-site model that contains strictly van der Waals interactions through the use of the Lennard-Jones potential. These parameters are adjusted to include implicit electrostatic and induction effects, allowing for accurate reproduction of bulk hydrogen data for densities up to the liquid range. The lack of such explicit effects, however, make this model of dubious utility in modeling interactions with both weakly and highly polar heterogeneous media where these forces produce significant contributions to the intermolecular energetics. Hence, the Buch model was used as a control. Note, as stated in the main text, the Buch model was able to describe the correct H<sub>2</sub> uptake in the MOM studied herein, as the small pore sizes of the MOM causes van der Waals energetics to dominate.

The BSS and BSSP models are five-site models that include van der Waals parameters on the center-of-mass site and off-atomic positions, and atomic point partial charges on the center-of-mass site and atomic positions.<sup>38</sup> These parameters differ, as the former has parameters adjusted to compensate for the lack of explicit induction while the latter includes additional atomic point polarizability parameters on the center-of-mass site and atomic positions. Moreover, the off-atomic positions are located 0.329 Å from the center-of-mass site in BSS, while such positions are shifted to 0.363 Å in BSSP. Both models reproduce experimental data in relatively nonpolar media such as MOF-5 where the contributions of many-body polarization are minor.<sup>7</sup> However, in highly charged/polar heterogeneous media, only the BSSP model has been shown to reproduce experiment data consistently.<sup>6,8</sup> The relative positions and parameters for all H<sub>2</sub> models are listed in Table 5. Note, the bulk H<sub>2</sub> pressure-density isotherms for the three hydrogen models compared to experimental data at 77 K and 298 K can be found in previous work.<sup>38,39</sup>

**Table 5.** Parameters used to characterize the Buch, BSS, and BSSP H<sub>2</sub> models. COM refers to the center-of-mass site, and OA refers to the off-atomic sites.

Model	Atomic Site	$r(\text{Å})$	$\epsilon(\text{K})$	$\sigma(\text{Å})$	$q (e^-)$	$\alpha^\circ(\text{Å}^3)$
Buch	COM	0.00000	34.20000	2.96000	0.00000	0.00000
BSS	COM	0.00000	8.85160	3.22930	-0.74640	0.00000
	H	0.37100	0.00000	0.00000	0.37320	0.00000
	H	-0.37100	0.00000	0.00000	0.37320	0.00000
	OA	0.32900	4.06590	2.34060	0.00000	0.00000
	OA	-0.32900	4.06590	2.34060	0.00000	0.00000
BSSP	COM	0.00000	12.76532	3.15528	-0.74640	0.69380
	H	0.37100	0.00000	0.00000	0.37320	0.00044
	H	-0.37100	0.00000	0.00000	0.37320	0.00044
	OA	0.36300	2.16726	2.37031	0.00000	0.00000
	OA	-0.36300	2.16726	2.37031	0.00000	0.00000

### N<sub>2</sub> Model

The N<sub>2</sub> model used in this study is a rigid five-site model that includes van der Waals and explicit charge-quadrupole interactions. Lennard-Jones parameters are located on the center-of-mass and atomic sites, and partial charges are located on the center-of-mass and off-atomic sites that extend 0.738 Å from the center-of-mass. As with the CO<sub>2</sub> models, this model was developed according to a previously reported procedure.<sup>38,39</sup> The parameters for this N<sub>2</sub> model can be found in Table 6.

Figure 5 shows the GCMC-calculated bulk N<sub>2</sub> pressure-density isotherms for the developed N<sub>2</sub> model compared to experimental data<sup>40</sup> at 77 K and up to 1.0 atm and 298 K and up to 100.0 atm. For this, the Peng-Robinson equation of state<sup>28</sup> was used to determine the chemical potential for N<sub>2</sub>. The isotherms for this model are in excellent agreement with the experimental data for the given pressure range at both temperatures to within joint uncertainties.

**Table 6.** Parameters used to characterize the N<sub>2</sub> model used in this work. COM refers to the center-of-mass site, and OA refers to the off-atomic sites.

Model	Atomic Site	$r(\text{Å})$	$\epsilon(\text{K})$	$\sigma(\text{Å})$	$q(e^-)$
N <sub>2</sub>	COM	0.00000	17.60293	3.44522	1.04742
	N	0.54900	0.00000	0.00000	-0.52371
	N	-0.54900	0.00000	0.00000	-0.52371
	OA	0.73800	18.12772	3.15125	0.00000
	OA	-0.73800	18.12772	3.15125	0.00000

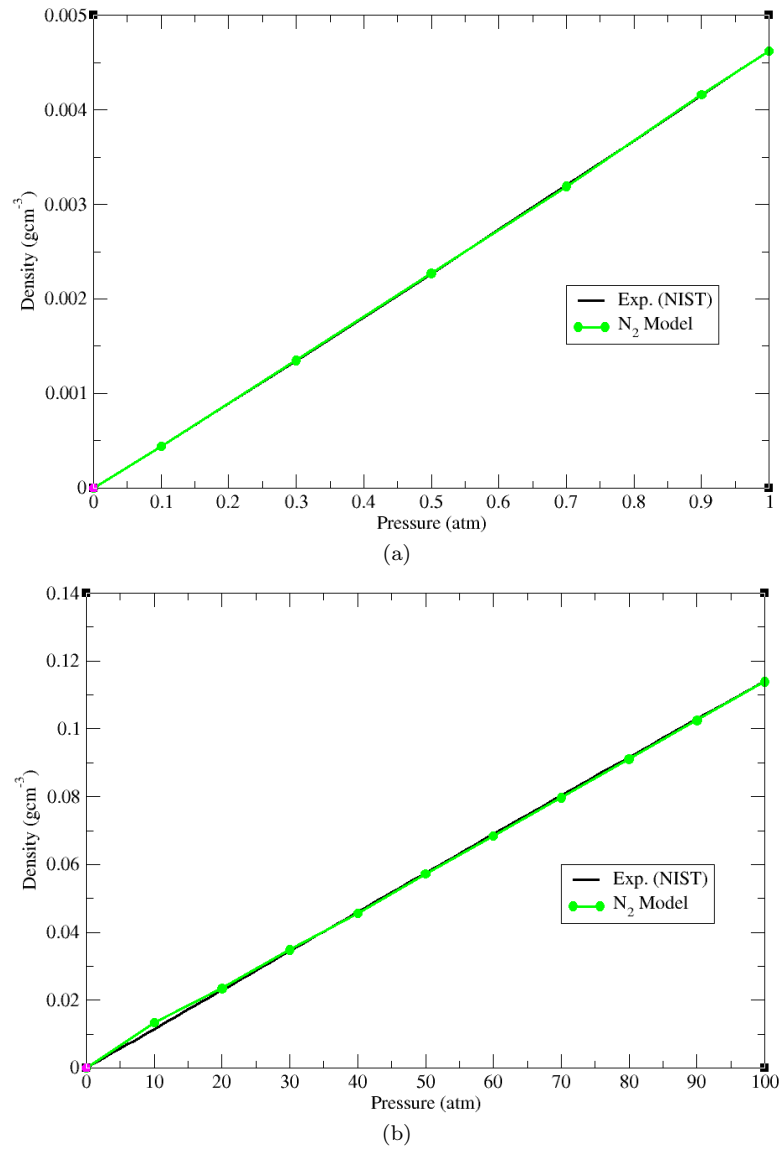


**Figure 5.** Pressure-density isotherm of  $N_2$  for the developed  $N_2$  model compared to experiment at (a) 77 K and up to 1.0 atm and (b) 298 K and up to 100.0 atm.

### Other Models

**Table 7.** Parameters used to characterize the Ar model<sup>41</sup> used in this work.

Model	Atomic Site	$r(\text{\AA})$	$\epsilon(\text{K})$	$\sigma(\text{\AA})$	$q(e^-)$
Ar	Ar	0.00000	93.09800	3.44600	0.00000

**Table 8.** Parameters used to characterize the CO model<sup>42</sup> used in this work. OA refers to the off-atomic sites.

Model	Atomic Site	$r(\text{\AA})$	$\epsilon(\text{K})$	$\sigma(\text{\AA})$	$q(e^-)$
CO	C	0.00000	39.90900	2.88500	0.83100
	O	1.12800	61.58460	2.88500	0.00000
	OA	-0.43700	0.00000	0.00000	-0.63600
	OA	0.97000	0.00000	0.00000	-0.19500

**Table 9.** Parameters used to characterize the TIP3P H<sub>2</sub>O model<sup>43</sup> used in this work.

Model	Atomic Site	$x(\text{\AA})$	$y(\text{\AA})$	$z(\text{\AA})$	$\epsilon(\text{K})$	$\sigma(\text{\AA})$	$q(e^-)$
TIP3P	O	0.00000	0.00000	0.00000	76.42000	3.15100	-0.83400
	H	-0.75700	-0.58600	0.00000	0.00000	0.00000	0.41700
	H	0.75700	-0.58600	0.00000	0.00000	0.00000	0.41700

**Table 10.** Parameters used to characterize the TraPPE CO<sub>2</sub> model<sup>44</sup> used in this work.

Model	Atomic Site	$r(\text{\AA})$	$\epsilon(\text{K})$	$\sigma(\text{\AA})$	$q(e^-)$
TraPPE	C	0.00000	27.00000	2.80000	0.70000
	O	1.16000	79.00000	3.05000	-0.35000
	O	-1.16000	79.00000	3.05000	-0.35000

### Experimental Gas Sorption Data

$[\text{Cu}(\text{dpa})_2\text{SiF}_6]$  and  $[\text{Cu}(\text{dpa})_2\text{SiF}_6\text{-i}]$  were synthesized and activated according to the procedure reported previously.<sup>45</sup> All  $\text{CO}_2$  and  $\text{H}_2$  sorption measurements were conducted on a Micromeritics ASAP 2020 surface area and porosity analyzer. The experimental  $\text{CO}_2$  sorption isotherms at 298 K and 273 K and  $\text{CO}_2$   $Q_{st}$  values in both compounds are shown in Figures 6 and 7, respectively. The experimental hydrogen sorption isotherms at 77 K and 87 K and  $\text{H}_2$   $Q_{st}$  values in both compounds are shown in Figures 8 and 9, respectively.

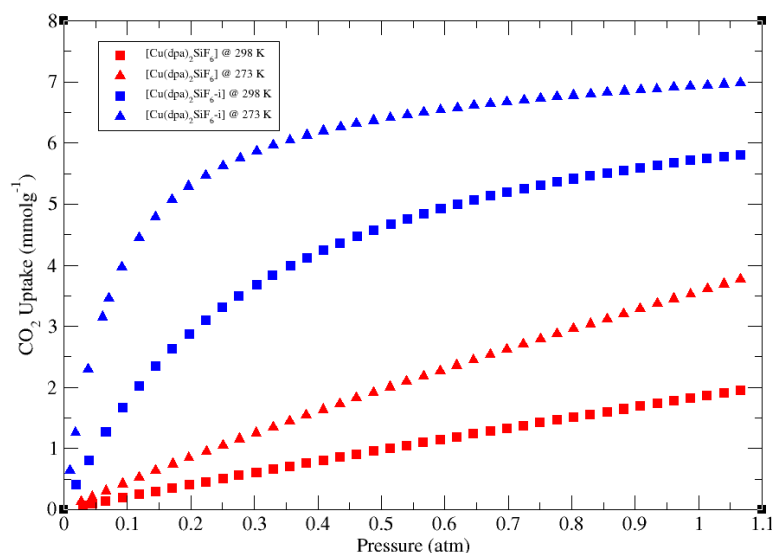


**Figure 6.** The experimental  $\text{CO}_2$  sorption isotherms at 298 K (squares) and 273 K (triangles) in  $[\text{Cu}(\text{dpa})_2\text{SiF}_6]$  (red) and  $[\text{Cu}(\text{dpa})_2\text{SiF}_6\text{-i}]$  (blue).

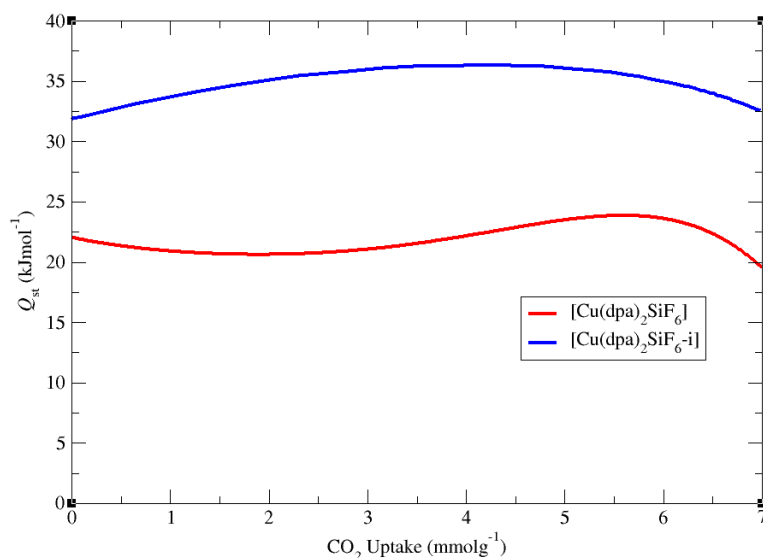


**Figure 7.** The experimental  $\text{CO}_2$   $Q_{st}$  values as a function of  $\text{H}_2$  uptake in  $[\text{Cu}(\text{dpa})_2\text{SiF}_6]$  (red) and  $[\text{Cu}(\text{dpa})_2\text{SiF}_6\text{-i}]$  (blue).

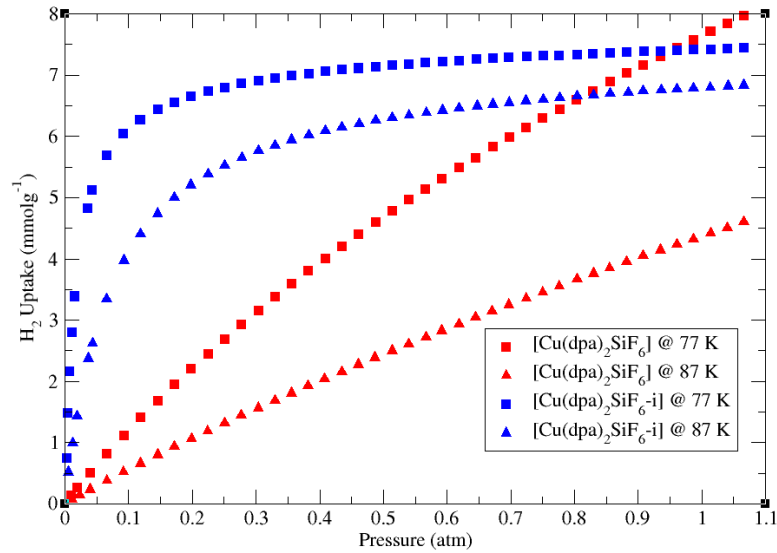


**Figure 8.** The experimental H<sub>2</sub> sorption isotherms at 77 K (squares) and 87 K (triangles) in [Cu(dpa)<sub>2</sub>SiF<sub>6</sub>] (red) and [Cu(dpa)<sub>2</sub>SiF<sub>6</sub>-i] (blue).

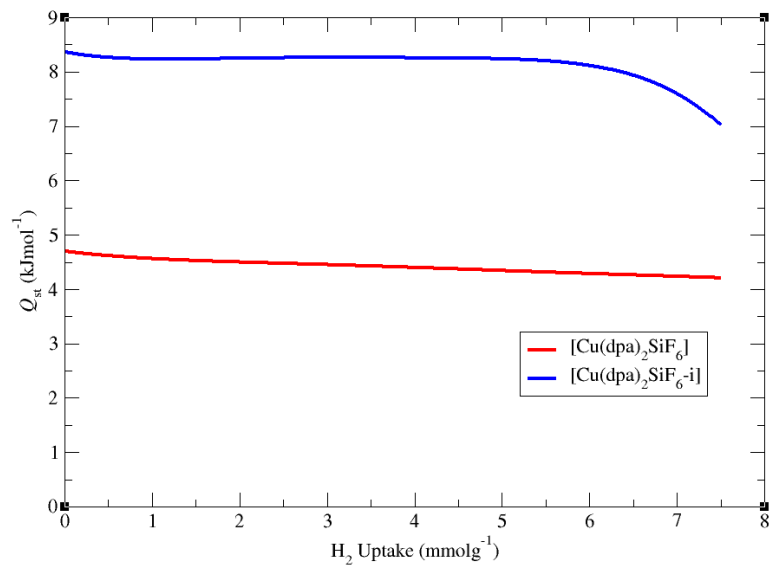


**Figure 9.** The experimental H<sub>2</sub>  $Q_{st}$  values as a function of H<sub>2</sub> uptake in [Cu(dpa)<sub>2</sub>SiF<sub>6</sub>] (red) and [Cu(dpa)<sub>2</sub>SiF<sub>6</sub>-i] (blue).

### Water Stability Test By Powder X-ray Diffraction

The as-synthesized crystals of  $[\text{Cu}(\text{dpa})_2\text{SiF}_6\text{-i}]$  were sequentially washed with methanol and then  $\text{H}_2\text{O}$ . To evaluate the water stability of  $[\text{Cu}(\text{dpa})_2\text{SiF}_6\text{-i}]$ , as-synthesized samples of the MOM (*ca.* 100 mg) were immersed in deionized water for as long as three weeks. Powder X-ray diffraction (PXRD) studies were then performed on the crystals. PXRD was carried out at room temperature on a Bruker D8 Advance  $\theta$ - $\theta$  diffractometer using  $\text{Cu-K}\alpha$  radiation ( $\lambda = 1.5418 \text{ \AA}$ ). Each scan spanned  $4^\circ$  to  $60^\circ$  in  $2\theta$  and required 4 minutes and 34 seconds to complete (step size =  $0.02^\circ$ ; step time = 0.1 s). The PXRD patterns reveal that there is essentially no change between the as-synthesized crystals and the crystals after immersion in water for three weeks (Figure 10). This demonstrates the remarkable water stability of  $[\text{Cu}(\text{dpa})_2\text{SiF}_6\text{-i}]$ .

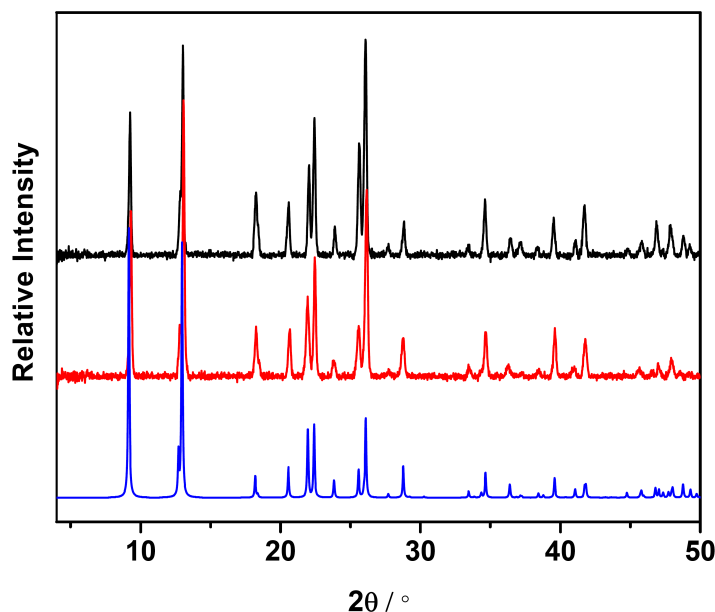


**Figure 10.** Powder X-ray diffraction (PXRD) patterns of  $[\text{Cu}(\text{dpa})_2\text{SiF}_6\text{-i}]$  for simulated plot (blue), as-synthesized sample (red), and water stability test after 3 weeks (black).

### Molecular Dynamics Simulation

NVE molecular dynamics (MD) simulation of the interactions of  $\text{CO}_2$  molecules in  $[\text{Cu}(\text{dpa})_2\text{SiF}_6\text{-i}]$  at 298 K was performed using an in-house modification of the LAMMPS (Large-scale Atomic/Molecular Massively Parallel Simulator) code<sup>46,47</sup> to include induced-dipole interactions. Various simulations were implemented on the MOM-sorbate system with a set number of  $\text{CO}_2^*$ -PHAST  $\text{CO}_2$  molecules. In all cases, the trajectories revealed that the  $\text{CO}_2$  molecules are indeed sorbed onto the equatorial fluorine atoms of the  $\text{SiF}_6^{2-}$  groups, with the molecules aligned in an alternating vertical–horizontal fashion with respect to the channel. Furthermore, it can be seen that the  $\text{CO}_2$  molecules can change its orientation as they are bound to the fluorine atoms, since there is room within the  $5.15 \text{ \AA}$  square channels to do so. However, the  $\text{CO}_2$  molecules will always try to orient themselves in a T-shaped manner because this a very favorable configuration of  $\text{CO}_2$  molecules in this MOM. A sample MD video showing this trajectory is given in the compressed folder for this manuscript.

## Additional Isotherms and Content

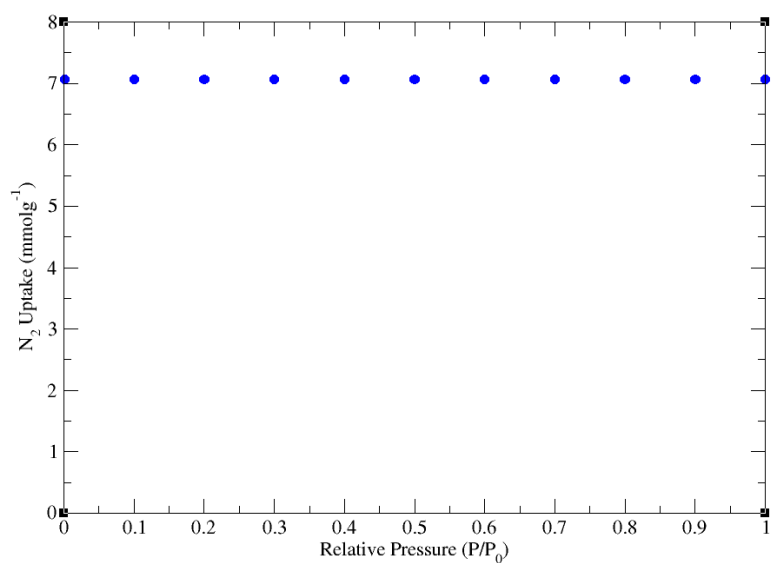


**Figure 11.** The simulated N<sub>2</sub> sorption isotherm at 77 K in [Cu(dpa)<sub>2</sub>SiF<sub>6</sub>-i]. The calculated N<sub>2</sub> uptake is 7.07 mmol g<sup>-1</sup> across all considered relative pressures.

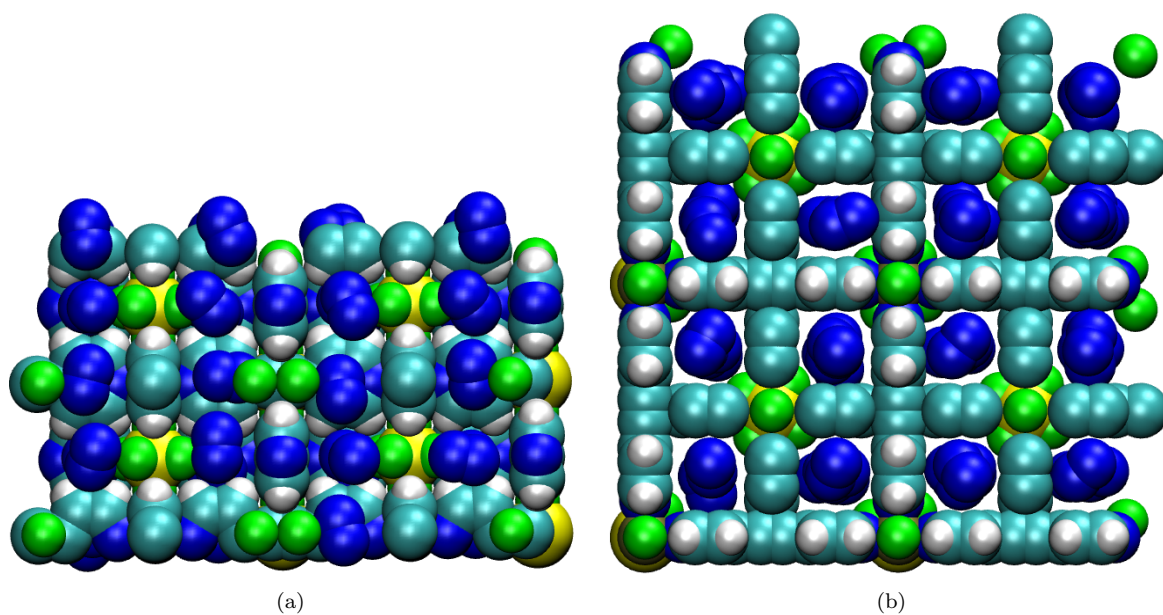


**Figure 12.** (a) The side view and (b) top view of the modeled  $2 \times 2 \times 2$  unit cell system of [Cu(dpa)<sub>2</sub>SiF<sub>6</sub>-i] at N<sub>2</sub> saturation with all atoms in their appropriate van der Waals radii. N<sub>2</sub> saturation corresponds to 8 N<sub>2</sub> molecules per unit cell. Atom colors: C = cyan, H = white, N = blue, F = green, Si = yellow, Cu = tan.

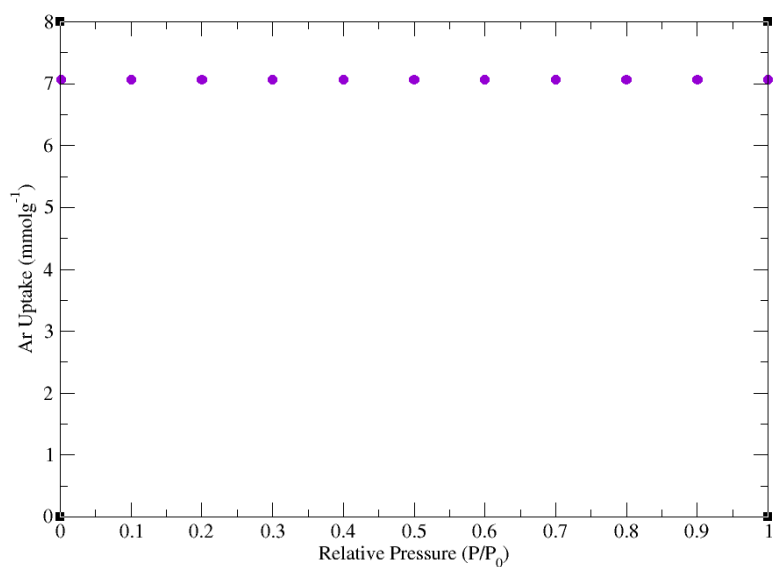


**Figure 13.** The simulated Ar sorption isotherm at 87 K in  $[\text{Cu}(\text{dpa})_2\text{SiF}_6\text{-i}]$ . The calculated Ar uptake is  $7.07 \text{ mmol g}^{-1}$  across all considered relative pressures

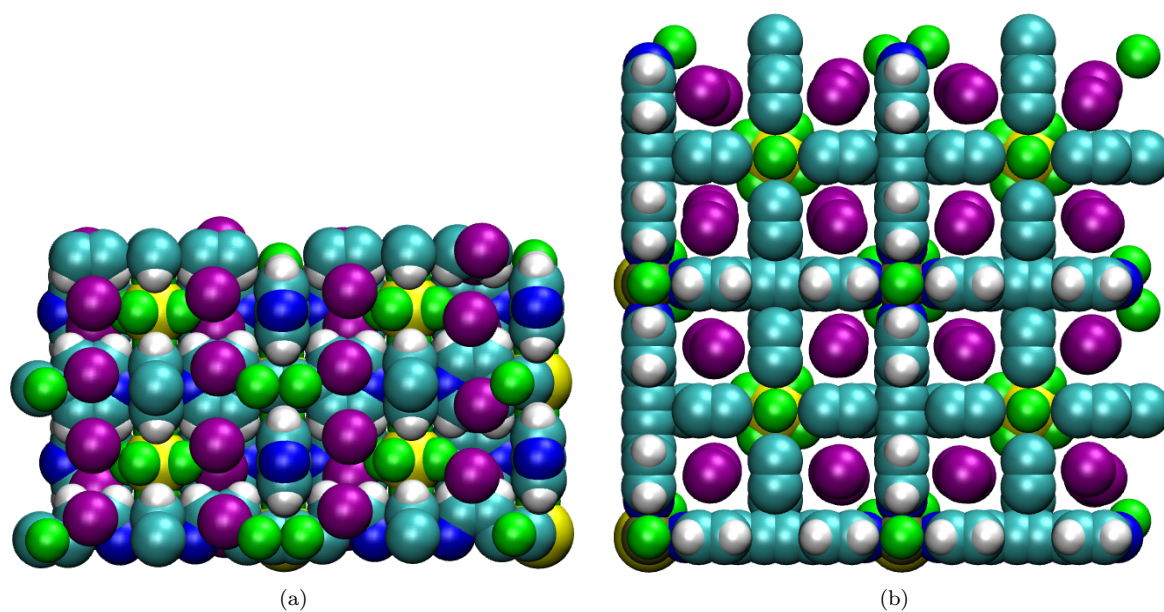


**Figure 14.** (a) The side view and (b) top view of the modeled  $2 \times 2 \times 2$  unit cell system of  $[\text{Cu}(\text{dpa})_2\text{SiF}_6\text{-i}]$  at Ar saturation with all atoms in their appropriate van der Waals radii. Ar saturation corresponds to 8 Ar atoms per unit cell. Atom colors: C = cyan, H = white, N = blue, F = green, Si = yellow, Cu = tan, Ar = violet.

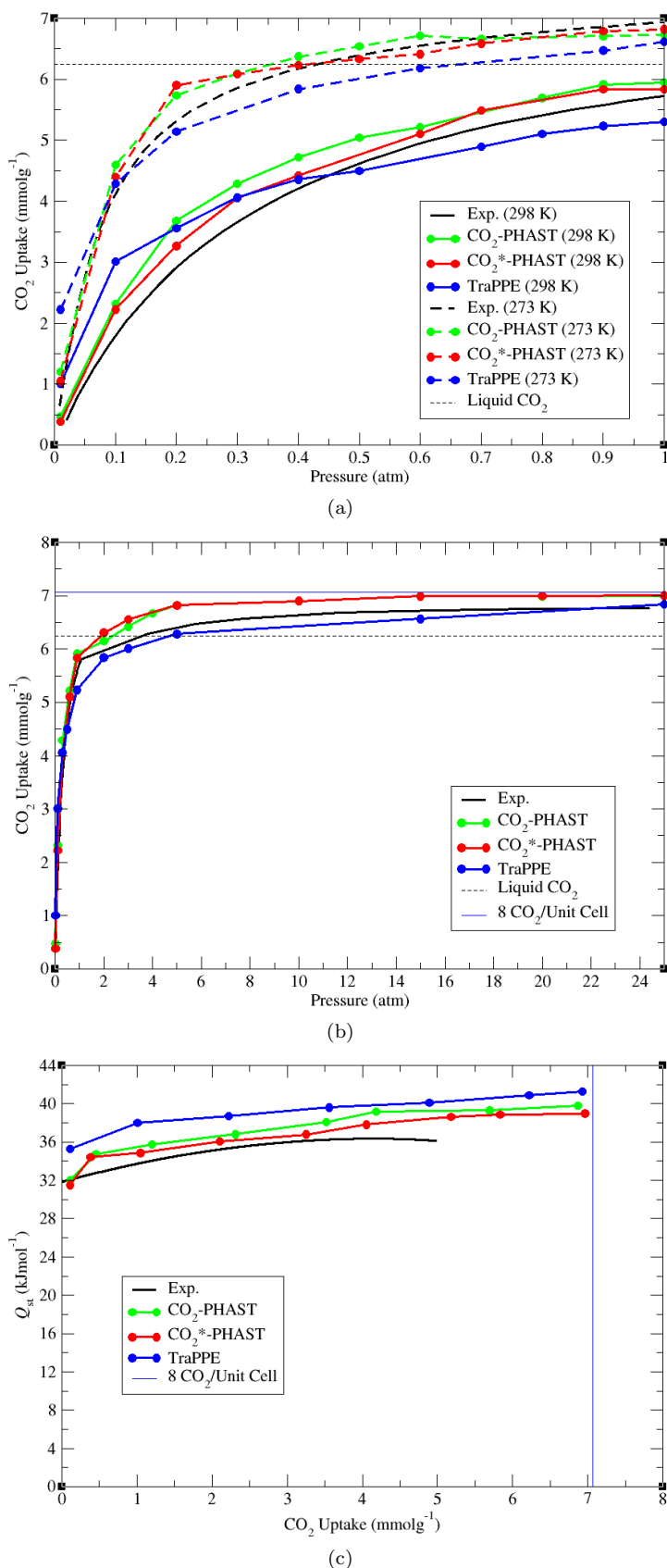


**Figure 15.** (a) Low-pressure (up to 1.0 atm) CO<sub>2</sub> sorption isotherms at 298 K (solid) and 273 K (dashed), (b) High-pressure (up to 25.0 atm) CO<sub>2</sub> sorption isotherms at 298 K, and (c) Isosteric heats of adsorption,  $Q_{st}$ , for CO<sub>2</sub> at 298 K plotted against CO<sub>2</sub> uptakes corresponding to pressures between 0 and 25.0 atm in [Cu(dpa)<sub>2</sub>SiF<sub>6</sub>-i] for experiment (black), CO<sub>2</sub>-PHAST model (green), CO<sub>2</sub>\*-PHAST model (red), and TraPPE model (blue). The dashed line represents the CO<sub>2</sub> uptake corresponding to liquid CO<sub>2</sub> density and the blue line represents the CO<sub>2</sub> uptake corresponding to CO<sub>2</sub> saturation (8 CO<sub>2</sub> molecules per unit cell).

- <sup>1</sup> Chen, D.-L.; Stern, A. C.; Space, B.; Johnson, J. K. *The Journal of Physical Chemistry A* **2010**, *114*, 10225–10233.
- <sup>2</sup> Watanabe, T.; Manz, T. A.; Sholl, D. S. *The Journal of Physical Chemistry C* **2011**, *115*, 4824–4836.
- <sup>3</sup> Stern, A. C.; Belof, J. L.; Space, B. *J. Chem. Phys.* **2012**, *136*, 034705.
- <sup>4</sup> Valiev, M.; Bylaska, E.; Govind, N.; Kowalski, K.; Straatsma, T.; Dam, H. V.; Wang, D.; Nieplocha, J.; Apra, E.; Windus, T.; de Jong, W. *Computer Physics Communications* **2010**, *181*, 1477 – 1489.
- <sup>5</sup> Cornell, W. D.; Cieplak, P.; Bayly, C. I.; Gould, I. R.; Merz, K. M.; Ferguson, D. M.; Spellmeyer, D. C.; Fox, T.; Caldwell, J. W.; Kollman, P. A. *Journal of the American Chemical Society* **1995**, *117*, 5179–5197.
- <sup>6</sup> Belof, J. L.; Stern, A. C.; Eddaoudi, M.; Space, B. *Journal of the American Chemical Society* **2007**, *129*, 15202–15210, PMID: 17999501.
- <sup>7</sup> Belof, J. L.; Stern, A. C.; Space, B. *The Journal of Physical Chemistry C* **2009**, *113*, 9316–9320.
- <sup>8</sup> Forrest, K. A.; Pham, T.; McLaughlin, K.; Belof, J. L.; Stern, A. C.; Zaworotko, M. J.; Space, B. *The Journal of Physical Chemistry C* **2012**, *116*, 15538–15549.
- <sup>9</sup> Stevens, W. J.; Basch, H.; Krauss, M. *J. Chem. Phys.* **1984**, *81*, 6026.
- <sup>10</sup> Hay, P. J.; Wadt, W. R. *J. Chem. Phys.* **1985**, *82*, 270.
- <sup>11</sup> LaJohn, L. A.; Christiansen, P. A.; Ross, R. B.; Atashroo, T.; Ermler, W. C. *J. Chem. Phys.* **1987**, *87*, 2812.
- <sup>12</sup> Chirlian, L. E.; Francl, M. M. *Journal of Computational Chemistry* **1987**, *8*, 894–905.
- <sup>13</sup> Breneman, C. M.; Wiberg, K. B. *Journal of Computational Chemistry* **1990**, *11*, 361–373.
- <sup>14</sup> Applequist, J.; Carl, J. R.; Fung, K.-K. *Journal of the American Chemical Society* **1972**, *94*, 2952–2960.
- <sup>15</sup> Thole, B. *Chemical Physics* **1981**, *59*, 341 – 350.
- <sup>16</sup> Bode, K. A.; Applequist, J. *The Journal of Physical Chemistry* **1996**, *100*, 17820–17824.
- <sup>17</sup> Belof, J. L. Ph.D. thesis, University of South Florida, 2009.
- <sup>18</sup> van Duijnen, P. T.; Swart, M. *The Journal of Physical Chemistry A* **1998**, *102*, 2399–2407.
- <sup>19</sup> Dinh, T.-L.; Huber, G. A. *Journal of Mathematical Modelling and Algorithms* **2005**, *4*, 111–128, 10.1007/s10852-004-3526-y.
- <sup>20</sup> Palmo, K.; Krimm, S. *Chemical Physics Letters* **2004**, *395*, 133–137.
- <sup>21</sup> DeVane, R.; Space, B.; Perry, A.; Neipert, C.; Ridley, C.; Keyes, T. *Journal of Chemical Physics* **2004**, *121*, 3688–3701.
- <sup>22</sup> Perry, A.; Neipert, C.; Space, B.; Moore, P. B. *Chemical Reviews* **2006**, *106*, 1234–1258, PMID: 16608179.
- <sup>23</sup> Shao, Y. et al. *Phys. Chem. Chem. Phys.* **2006**, *8*, 3172.
- <sup>24</sup> Belof, J. L.; Space, B. *Massively Parallel Monte Carlo (MPMC)*, Available on Google Code, 2012.
- <sup>25</sup> Metropolis, N.; Rosenbluth, A. W.; Rosenbluth, M. N.; Teller, A. H.; Teller, E. *Phys. Lett. B* **1953**, *21*, 1087–1092.
- <sup>26</sup> McQuarrie, D. A. *Statistical Mechanics*; University Science Books: Sausalito, CA, 2000; Chapt. 3, pg. 53.
- <sup>27</sup> Frenkel, D.; Smit, B. *Understanding Molecular Simulation: From Algorithms to Applications*; Academic Press: New York, 2002; Chapt. 5, Sect. 6.1, p.129.
- <sup>28</sup> Peng, D.-Y.; Robinson, D. B. *Industrial and Engineering Chemistry Fundamentals* **1976**, *15*, 59–64.
- <sup>29</sup> Boublik, T. *Fluid Phase Equil.* **2005**, *240*, 96–100.
- <sup>30</sup> Ewald, P. P. *Annalen der Physik* **1921**, *369*, 253–287.
- <sup>31</sup> Fennell, C. J.; Gezelter, J. D. *Journal of Chemical Physics* **2006**, *124*, 234104.
- <sup>32</sup> Feynman, R. P.; Hibbs, A. R. *Quantum Mechanics and Path Integrals*; McGraw-Hill: New York, 1965; Chapt. 10, Sect. 3, pg. 281.
- <sup>33</sup> Siperstein, F.; Myers, A.; Talu, O. *Molecular Physics* **2002**, *100*, 2025–2030.
- <sup>34</sup> Wolf, D.; Keblinski, P.; Phillpot, S. R.; Eggebrecht, J. *Journal of Chemical Physics* **1999**, *110*, 8254.
- <sup>35</sup> Nicholson, D.; Parsonage, N. G. *Computer Simulation and the Statistical Mechanics of Adsorption*; Academic Press: London, 1982.
- <sup>36</sup> Angus, S.; Armstrong, B.; de Reuck, K. M. *International Thermodynamic Tables of the Fluid State: Carbon dioxide*; Pergamon Press: Oxford, United Kingdom, 1976; Vol. 3, pp 68–76.
- <sup>37</sup> Buch, V. *J. Chem. Phys.* **1994**, *100*, 7610–7629.
- <sup>38</sup> Belof, J. L.; Stern, A. C.; Space, B. *Journal of Chemical Theory and Computation* **2008**, *4*, 1332–1337.
- <sup>39</sup> McLaughlin, K.; Cioce, C. R.; Belof, J. L.; Space, B. *J. Chem. Phys.* **2012**, *136*, 194302.
- <sup>40</sup> Lemmon, E.; McLinden, M.; Friend, D. In *NIST Chemistry WebBook*; Linstrom, P.; Mallard, W., Eds.; National Institute of Standards and Technology: Gaithersburg, MD, 2005, Vol. 69, <http://webbook.nist.gov>.
- <sup>41</sup> Rappé, A. K.; Casewit, C. J.; Colwell, K. S.; Goddard, W. A.; Skiff, W. M. *Journal of the American Chemical Society* **1992**, *114*, 10024–10035.
- <sup>42</sup> Piper, J.; Morrison, J. A.; Peters, C. *Molecular Physics* **1984**, *53*, 1463–1480.
- <sup>43</sup> Jorgensen, W. L.; Chandrasekhar, J.; Madura, J. D.; Impey, R. W.; Klein, M. L. *J. Chem. Phys.* **1983**, *79*, 926.
- <sup>44</sup> Potoff, J. J.; Siepmann, J. I. *AIChE Journal* **2001**, *47*, 1676–1682.
- <sup>45</sup> Nugent, P.; Belmabkhout, Y.; Burd, S. D.; Cairns, A. J.; Luebke, R.; Forrest, K.; Pham, T.; Ma, S.; Space, B.; Wojtas, L.; Eddaoudi, M.; Zaworotko, M. J. *Nature* **2013**, *495*, 80–84.
- <sup>46</sup> Plimpton, S. et al. *Journal of Computational Physics* **1995**, *117*, 1–19.
- <sup>47</sup> Hogan, A.; Space, B. *LAMMPS Induced-Dipole Polarization Pair Style*, Available on Google Code, 2013.